15TH IEA HEAT PUMP CONFERENCE
MAY 26–29, 2026 | HOFBURG
VIENNA 2026
DECARBONISATION THROUGH INNOVATION

Design and experimental characterization of a multi-layout R1233zd(E) high temperature heat pump

A Zini [a*], E. Prataviera [b], A. Debattisti [b], L Talluri [a], F. Poletto [b], and A Rocchetti [a]

[a] Thermodynamics and Heat Transfer Research Group – Department of Industrial Engineering, University of Florence (Italy)
[b] HiRef Spa, Tribano, Padova (Italy)

Abstract

A 40 kW high temperature heat pump for thermal upgrade up to 130°C has been developed and experimentally tested as part of the THUNDER Horizon EU project, which focuses on an innovative approach to data centre waste heat reutilisation. Security constraints imposed by data centre operators required the use of an A1 working fluid. R1233zd(E) has been selected for its safety, lack of GWP limitations and low PFAS-related issues. A preliminary numerical model was developed to support the selection of the main components and to provide an initial assessment of the expected performance variations under different system layouts. This approach enabled a more efficient experimental design, helping to identify the most promising configurations for maximizing the heat pump efficiency. The device has been equipped with a highly flexible scroll compressor and two performance-enhancing components, such as an economiser and an internal regenerative heat exchanger. Different layouts and the influence of these two heat exchangers have therefore been experimentally tested, varying the temperature lift at different evaporation levels. Even though the use of a regenerative internal heat exchanger is not mandatory considering the shape of the saturation curve, to avoid wet compression, its use can improve device performance up to 5%. A similar effect is observed when the economizer is included in the circuit, while the combined use of both heat exchangers can increase the COP up to 9.5%.

Keywords: High Temperature Heat Pump, Waste Heat Recovery, Economiser, Internal Heat Exchanger, Thermochemical storage

1. Introduction

Data centre active cooling is a valuable source of waste heat that is commonly discharged into the environment. Its recovery is of paramount importance to lower global greenhouse gases emissions [1]. The constraint to the reutilisation of DC-WH is related to its low thermal level (rejection temperatures in the range of 30–40 °C, depending on external temperatures and type of cooling media), so its integration, to support different type of end-users, involves the use of devices, such HP, capable of raising this level to that required by the specific application. In industrial processes requiring heat at temperatures above 100°C, HTHPs must be considered, in which tailored working fluids and system layouts are specifically designed to address the challenges that arise when a reverse cycle operates at high condensation temperature levels [2]. The nearly constant annual thermal output of DC cooling systems [3] and the need for active summer cooling, create challenges when using DC-WH for applications requiring heat only in winter. This occurs in building heating or DHNs, which have strong seasonal demand peaks in winter. The mismatch limits direct WH use, as surplus heat in warmer months must be stored through seasonal TES.

An innovative system concept for sustainable waste heat recovery and seasonal thermal storage tailored for data centres in urban environments has been proposed in the context of the THUNDER project [4]. Low-grade

* Corresponding author. Tel.: +39 3804337930
E-mail address: andrea.zini@unifi.it

waste heat from data centre active cooling is harnessed during summer and stored using thermochemical material-based TES; leveraging on reversible chemical reactions (endothermic during charging and exothermic during discharging) this approach offers a promising alternative to sensible and latent TES technologies, providing significantly higher energy densities. However, two key challenges arise with the use of this technology, depending on the type of TCM employed: the charging temperatures can be relatively high (even exceeding 100 °C), and the heat released during the discharging phase may occur at a relatively low thermal level. During periods of high thermal energy demand, the stored heat is discharged into a DHN.

To meet the required thermal levels, a highly flexible HTHP is thus required, ideally providing performances as stable as possible over a wide temperature range, supported by a simple yet effective layout.

In Figure 1 the THUDNER concept design is shown with all the important thermal levels involved. The DC active cooling device (labelled as “A”) simultaneously provides the required cooling capacity to the servers and a first thermal upgrade step, recovering the WH to supply the HTHP (labelled as “B”). This device is directly connected to the TCM – TES system to perform its charging during the summer months, providing the heat required by the endothermic desorption process of TCM. If the storage device is not connected to the system during some summer days, the storage tank ensures the decoupling of the two boosting stages, facilitating the heat dissipation at the lower condenser into the environment through a dry cooler. The discharging process (less demanding in terms of condensation temperature levels), is managed by the same HTHP (labelled as “C” only for Figure 1 visualisation purposes); the working fluid evaporates by absorbing heat from the TCM exothermic absorption process and performs an upgrade of its thermal level to those needed to feed the DHN lines.

Thermal upgrade practice plays a pivotal role in the energy chain, significantly influencing the overall system efficiency. If characteristic temperature levels are varied, the performance of all the device’s changes.

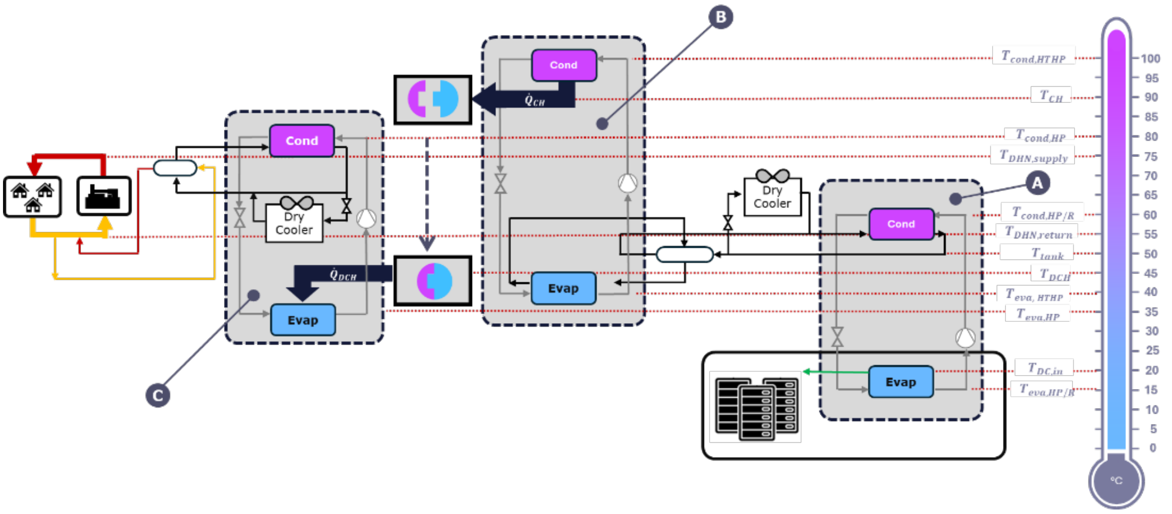

Figure 1: THUNDER project WHR concept design

This study aims to design and assess HTHP concept suitable for integration with a TCM based seasonal TES system. The research focused on enabling efficient heat delivery above 120 °C, a key requirement for thermochemical materials and industrial applications. To achieve this, an advanced cycle architecture was conceived, incorporating auxiliary components such as an economiser and an internal regenerative heat exchanger to enhance thermal performance and system stability. The work combined detailed numerical modelling with experimental testing on a prototype unit, allowing validation of the proposed design approach and providing insights into the operational behaviour, integration potential, and applicability of the HTHP within innovative high-temperature energy systems.

2. Materials and methods

2.1. Working fluid preliminary selection

The optimal working fluid selection depends on the specific application [2]. Unfortunately, the fluids that exhibit the best characteristics for given temperature ranges involved in this study are also those with the most significant safety issues. DC companies often strongly oppose the installation of devices with safety issues related to both flammability and toxicity. The choice must therefore necessarily fall on fluids with an A1 safety classification. Excluding water (R718), whose use is technically challenging for the given temperature ranges, the A1-classified fluids operating in a subcritical cycle are only fluorinated synthetic fluids. Despite the selection already implying the use of fluids approved under the F-Gas regulation concerning GWP (and ODP) limitations, these fluids pose an additional issue, one not yet effectively regulated, related to PFAS production [5,6]. R1233zd(E) has been choice as the potential candidate for HTHP due to only a 2% of TFA molar yield from degradation compared to the 100% of R1224yd(Z) and around 20% of R1336mzz(Z) [7,8].

2.2. Numerical thermodynamic model

Especially in HTHP applications, the basic/standard configuration consisting of only four components (evaporator, compressor, condenser, and expansion valve) is not always feasible. Additional components such as an economiser (ECO) or a regenerative internal heat exchanger (IHX) help address two key challenges: limiting the compressor discharge temperature, which is limited to 170°C according to manufacturer data sheets and preventing wet compression, which can occur with so-called "skewed" working fluids.

Figure 2 shows the layout enabling the thermodynamic analysis of five different configurations (bleeding percentages are labelled as "y_i" with i from 1 to 4; in this study all the bleeding percentages related to the internal regenerative heat exchanger are strictly 0%, which means fully closed or 100%, which means fully open):

- STD layout: all the bleedings are fully closed
- ECO layout: all the bleedings are closed except for y_2
- IHX layout: y_4 and y_1 (or alternatively y_3) are fully open while y_2 is fully closed
- IHX+ECO layout: y_4 is fully open to activate the IHX on the cold vapour side, y1 is fully open to activate the IHX on the hot liquid side before the ECO, y_2 is open to activate the ECO, while y_3 is fully closed.
- ECO+IHX layout: y_4 is fully open to activate the IHX on the cold vapour side, y_2 is open to activate the ECO, y_3 is fully open to activate the IHX on the hot liquid side after the ECO, while y_1 is fully closed.

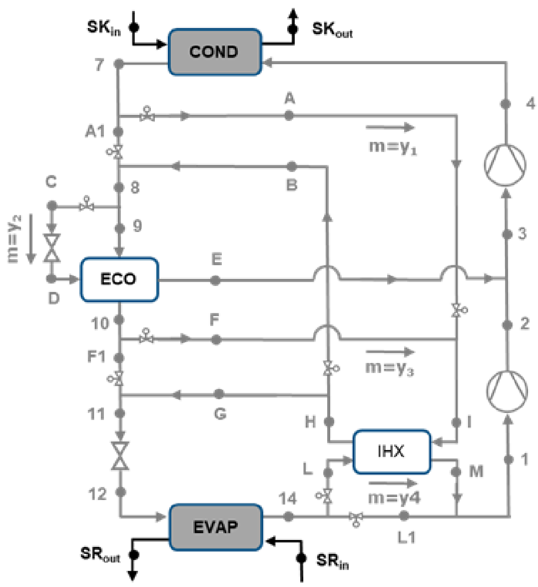

Figura 2: HTHP layout

The thermodynamic simulation was conducted in Python, with thermodynamic properties retrieved from REFPROP v10 [9]. The following assumptions were made for the simulation: steady state operations, no heat exchange between components and surroundings, no pressure losses in heat exchangers and pipes, constant heat rate of 38 kW delivered at the condenser, fixed compressor isentropic efficiency of 0.75, fixed IHX effectiveness of 0.3, The imposed conditions inside the heat exchangers are detailed in Table 1.

Table 1: Imposed conditions inside the heat exchangers

Physical quantity	Abbreviation	Value
Source temperature difference	ΔT_{SR}	5 K
Sink temperature difference	ΔT_{SK}	10 K
Temperature difference between sink outlet and condensation level	ΔT_{cond}	5 K
Temperature difference between source outlet and evaporation level	ΔT_{evap}	5 K
Useful superheating inside the evaporator	$\Delta T_{SH,u}$	5K
Useful subcooling inside the condenser	$\Delta T_{SC,u}$	0 K

Evaporation and condensation temperature levels were calculated based on the following equations:

$$T_{evap} = T_{SR,out} - \Delta T_{evap} \tag{1}$$

$$T_{cond} = T_{SK,out} + \Delta T_{cond} \tag{2}$$

The outflows from the IHX (when active) were calculated by imposing a fixed Kays&London effectiveness of 0.3 according to equations (3) and (4) if the maximum thermal capacity was the one of the hot liquid flow $(C_I > C_L)$ or alternatively according to equations (5) and (6) for the opposite condition $(C_I < C_L)$

$$h_M = h_L + \varepsilon \cdot cp_L \cdot (T_I - T_L) \tag{3}$$

$$h_H = h_I - \left(\frac{m_I}{m_L}\right) \cdot (h_I - h_H) \tag{4}$$

$$h_H = h_I - \varepsilon \cdot cp_I \cdot (T_I - T_L) \tag{5}$$

$$h_M = h_L + \left(\frac{m_I}{m_L}\right) \cdot (h_I - h_H) \tag{6}$$

Outlet conditions of the main flow inside the economiser (point “10” in Figure 2) were calculated applying energy and mass balances and considering the available cooling capacity of the diverted flow (point “E” in Figure 2) as a complete evaporation process, meaning that the diverted outflow from the economiser is in saturation conditions.

The pressure of the second flow at the economiser (point “E” in Figure 2) has been set in all the analysis according to the equation (7) fixing (or varying for parametric analysis) the value of j.

$$p_{ECO} = p_{evap} + j \cdot (p_{cond} - p_{evap}) \tag{7}$$

The COP was calculated as the ratio of the condenser thermal power and the total work rate absorbed by the compressors as stated in equation (8).

$$COP = \frac{\dot{Q}_{cond}}{\dot{W}_{comp}} = \frac{\dot{Q}_{cond}}{\dot{W}_{comp,1} + \dot{W}_{comp,2}} \tag{8}$$

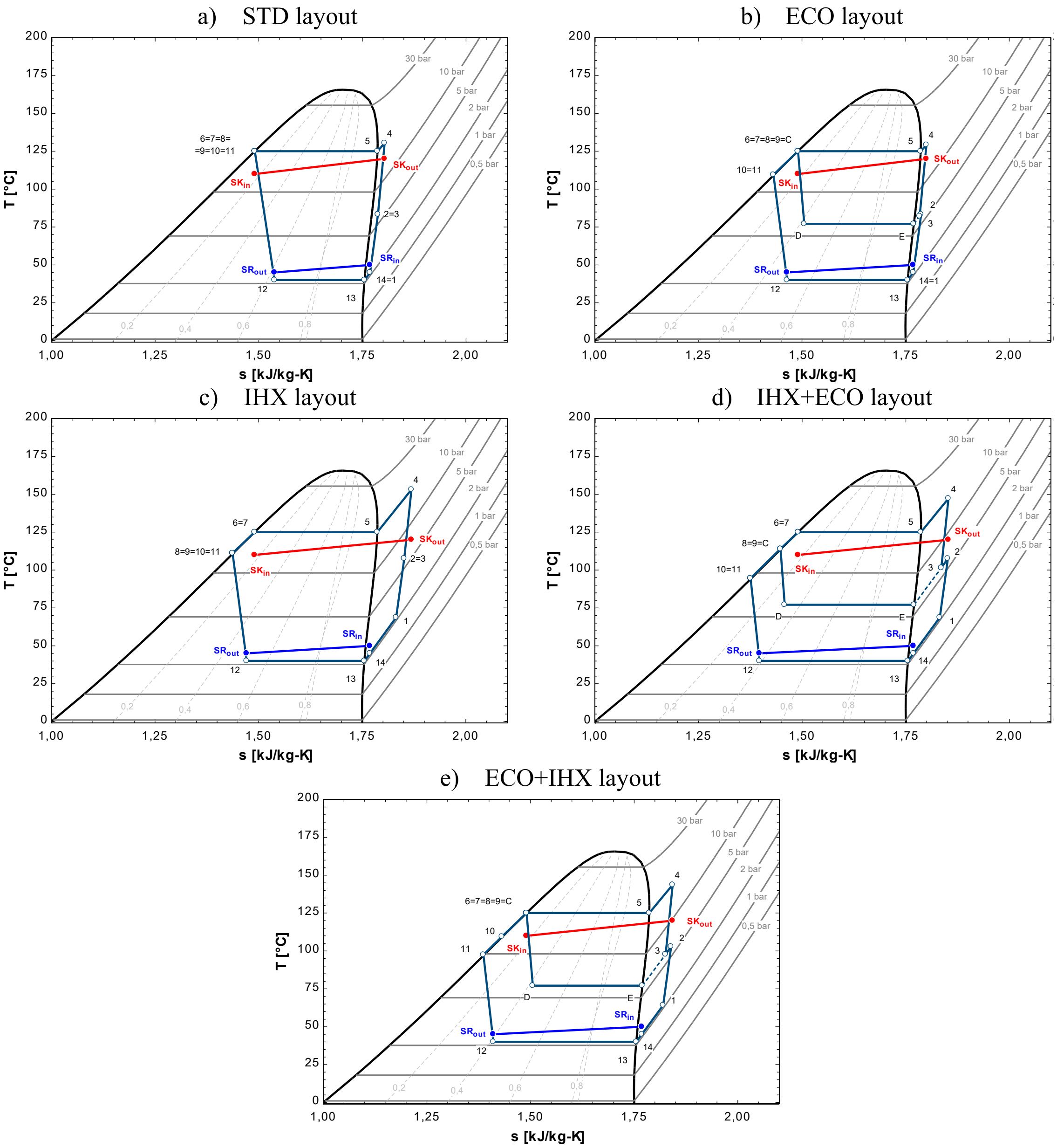

Figure 3: T-s diagrams for all the five HTHP layouts with R1233zd(E) as working fluid

2.3. Design and experimental set-up

The HTHP has been designed, realised and tested at HiRef S.p.A. facility. Figure 4 shows the 3D picture of this device and a photo of the unit after the completion of the manufacturing process, taken during the initial testing phase. The unit was then tested in a dedicated laboratory, using certified measurement equipment according to ISO EN 14511-3. The testing apparatus is represented in Figure 5. The setpoint temperature of the tank (maintained by an external dry cooler or chiller) corresponds to the temperature needed at the inlet of the source side (evaporator inlet). On the condenser side, a separate circuit with a tank internal heat exchanger allows water pressurization to exceed 100 °C. Hot water setpoint temperature is reached in this circuit by recirculating water with a three-way valve until reaching setpoint. Since HTHP will have to operate under highly variable boundary conditions, the testing procedure was designed to vary the sink water temperature from 70 °C to 130 °C and the source water temperature from 35 °C to 65 °C.

Figure 4: 3D CAD picture of the HTHP (left) and photo of the HTHP during testing (right)

The following temperatures and relative pressure probes have been installed in the refrigerant circuit during the tests (see Figure 2): 1, 4, 7, 10, 5 (only p), 14, E, G (only T). Pressure is logged using relative pressure probes with an uncertainty of ±1 %; temperature is instead logged using type T thermocouples (±0.2 °C), installed on the outlet side of the pipe using thermal paste. Inlet and outlet temperature of the source and sink fluid is measured with pt100 thermistors (±0.15 °C), while water flow rate is read using a magnetic volumetric flow rate meter on both hot and cold side. In any case it is worth mentioning that hot water flow reading was disturbed in some tests probably due to air bubbles in the closed circuit. For this reason, cooling capacity measurement is considered more reliable during data analysis. Acquisition hardware records every 4 seconds. Electric power is measured with separate electric grid analysers (±1 %) for pumps and compressor supply. Compressor power is measured before inverter. Inverter efficiency is assumed to be 0.95 for data analysis.

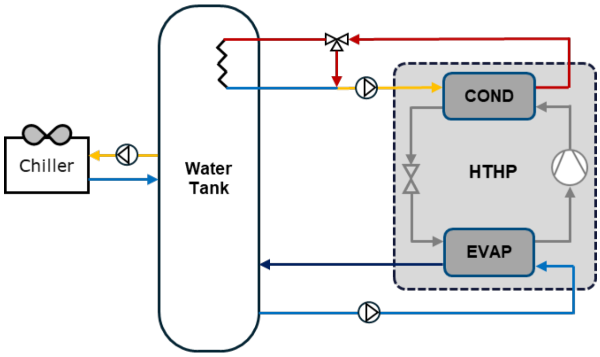

Figure 5: HTHP experimental test rig

Testing conditions are replicated for three refrigerant cycle configurations: STD, ECO, ECO+IHX. All thermodynamic points are tested controlling the expansion valve with superheating after the evaporator. A subset of points is then tested afterwards controlling superheating after the regenerator. (POST config). In all testing conditions compressor frequency is set to 85 Hz.

All parameters described in the previous sections are logged continuously during the tests. Data analysis started with an initial data filtering with the goal of selecting suitable and stable time slots for stable and reasonable conditions. After filtering stable time slots, averages are calculated for each measured value during defined time slots. Considering averages temperatures, cooling capacity is then calculated according to equation (9)

$$\dot{Q} = G_{SR} \cdot c_{p;SR} \cdot \rho_{SR} \cdot (T_{SR,in} - T_{SR,out}) \tag{9}$$

Evaporator refrigerant mass flow rate is instead calculated with the division of cooling capacity by the inlet and outlet enthalpy (from REFPROP v10 [9]).

3. Results and discussion

3.1. Numerical evaluation of the benefits of including additional components to the standard layout

Figure 6 illustrates the variation in COP as a function of the secondary flow pressure of the ECO expressed as a percentage (j) for different extracted fractions (y_2) for fixed evaporation and condensation thermal levels ($T_{evap} = 30\ °C; T_{cond} = 95°C$). The COP increases with rising ECO pressure and with a greater extracted fraction. Minimising throttling (i.e., maintaining the ECO pressure close to that of the condenser) has a more significant impact at higher extracted fractions.

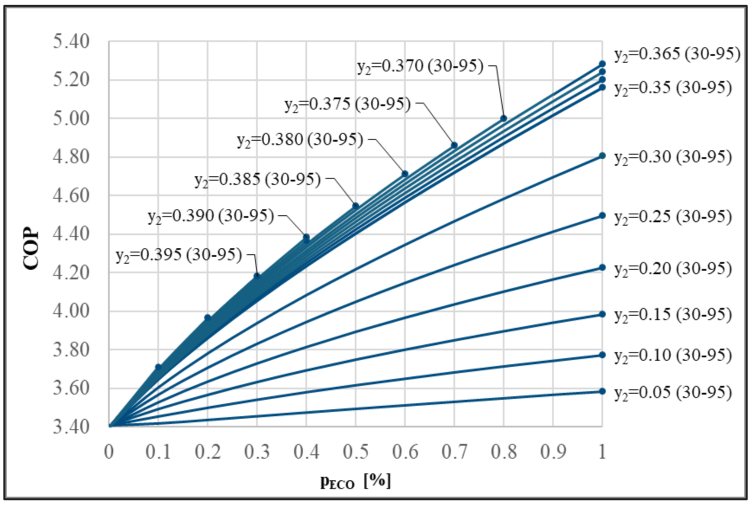

Figure 6: COP trends as a function of the percentage pressure at the economiser (properly j expressed in equation (7)) for different extracted fractions.

These COP trends are due to the reduction in mechanical power absorbed by the compressor. This reduction results from the combined contributions of the two stages. The power absorbed by the 1st stage increases as the ECO pressure rises—this is evident, as a greater portion of the total β is assigned to the 1st stage. However, it decreases with an increase in the extracted fraction. This occurs because, although the kJ/kg value remains unchanged, the primary mass flow directed towards the evaporator is reduced, consequently lowering the flow rate to the 1st stage as well. The power absorbed by the 2nd stage decreases as the ECO pressure rises. When this pressure is close to that of the evaporator, most of the total β is handled by the 2nd stage. Conversely, when the ECO pressure approaches that of the condenser, the 1st stage absorbs most of the total compression work. However, the power absorbed by the second stage is not affected by variations in the extracted flow rate (y_2), as this flow is reintroduced downstream of the 2nd stage suction (see Figure 7a).

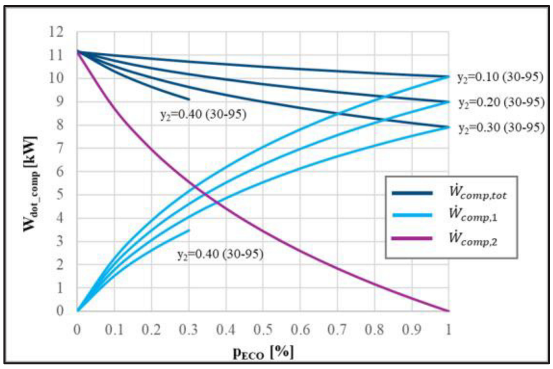

a)

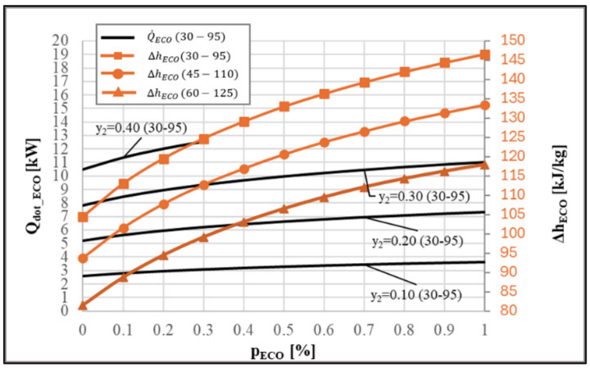

b)

Figure 7: a) Power absorbed by the compressors (total and individual terms) b) Thermal power exchanged in the economiser and latent fraction available after the expansion of the extracted flow, as a function of the percentage pressure at the economiser for different extracted fractions

The extracted fraction (y_2) influences the maximum pressure allowable at the ECO. As y_2 increases, greater throttling is required, resulting in a further deviation from the condenser pressure. Minimising throttling (with j approaching 1, causing the ECO pressure to approach that of the condenser) increases the available latent heat of evaporation: this occurs because the quality at point D decreases as j increases, despite the narrowing of the two-phase region as it shifts towards the critical pressure. Both quantities are dimensionless and remain unaffected by the extracted fraction (see Figure 7b). The thermal power harnessed in the ECO to provide subcooling for the main flow is determined by the product of the available latent heat and the extracted mass flow rate. This power increases with both variables: with ECO pressure, as the latent heat fraction rises, and with y_2, as the mass flow rate increases (see Figure 7b). This explains the reduction in the maximum throttling limit: the thermal power made available to the economiser would be sufficient to subcool the primary flow below the evaporation temperature.

The analysis has been also conducted by shifting the cycle upward by 15 K while maintaining the same gross temperature lift for two additional pairs of evaporation/condensation conditions (45-110 °C and 60-125 °C). This results in an increase of the maximum fraction that can be extracted (y_2). Additionally, the limit on maximum ECO pressure is reached later for the same diverted flow rate. This is because, when shifting the cycle upward, the latent heat of vaporization available in the ECO decreases (see Figure 10b) Consequently, for the same heat exchange power in the ECO, more mass flow rate can be extracted before reaching the limit on the inlet temperature at the expansion valve (which must, of course, be higher than the imposed evaporation temperature).

Using a regenerative heat exchanger (IHX) improves HTHP performances. Focusing on the condition 30-95 °C (Figure 8) as fixed evaporation and condensation thermal levels, at low extraction rates, the position of the IHX has a negligible impact (although using the IHX is still recommended). As the extraction rate increases (increasing y_2), placing the IHX after the ECO becomes almost useless, as it results in the same outcome as using only the ECO. This is because the entire available subcooling is practically saturated by the ECO, leaving no room for the IHX. However, placing the IHX before the ECO reduces the maximum extractable fraction, as an initial subcooling is already achieved in the IHX. The influence of the IHX increases with rising condensation temperature.

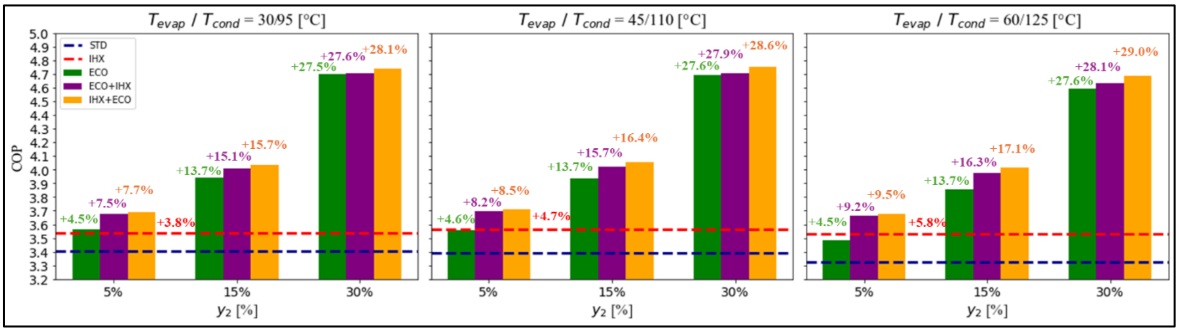

Figure 8: Variation of the COP for different layouts for three extracted fractions at three different evaporation and condensation temperatures

3.2. Experimental results

Figure 9 shows the comparison between measures and compressor manufacturer polynomials for electric consumption, cooling capacity and evaporator mass flow rate. Electricity consumption errors are typically lower than 15%, and they are always overestimated by manufacturer polynomials. In few cases the error is larger when the sink outlet temperature reaches very high values (around 135 °C). Concerning cooling capacity, the trend is similar and usually overestimated by polynomials. It is worth mentioning that a correction is applied to correct the cooling capacity and evaporator reference mass flow rate based on the real superheating and subcooling. The correction consists of considering a corrected value of evaporator enthalpy inlet/outlet difference considering the difference between measured and polynomial assumption on superheating and subcooling. This difference is then used to change both parameters accordingly to compare polynomial results with real data. Despite this correction allows a better comparison, it considers only the enthalpy difference between a similar cycle with a change in superheating and subcooling, and it does not consider any other difference than can occur in a real condition where superheating and subcooling are different (as a different evaporator or condensing temperature, different regenerator behaviour, etc.). This is one of the reasons why few points result in a larger difference between polynomial and measured cooling capacity. Another explanation of this difference could be due to an unstable condition of the economizer valve (even after initial data filtering). This behaviour is even larger in evaporator mass flow rate comparison, as this parameter is also affected by the uncertainty in the temperature measurement on the outlet pipe (that affects enthalpy calculation). Despite the difficulty in comparing measures with compressor manufacturer estimation, data seems to follow coherently polynomials, even though both measured electricity consumption and cooling capacity are generally slightly lower than model.

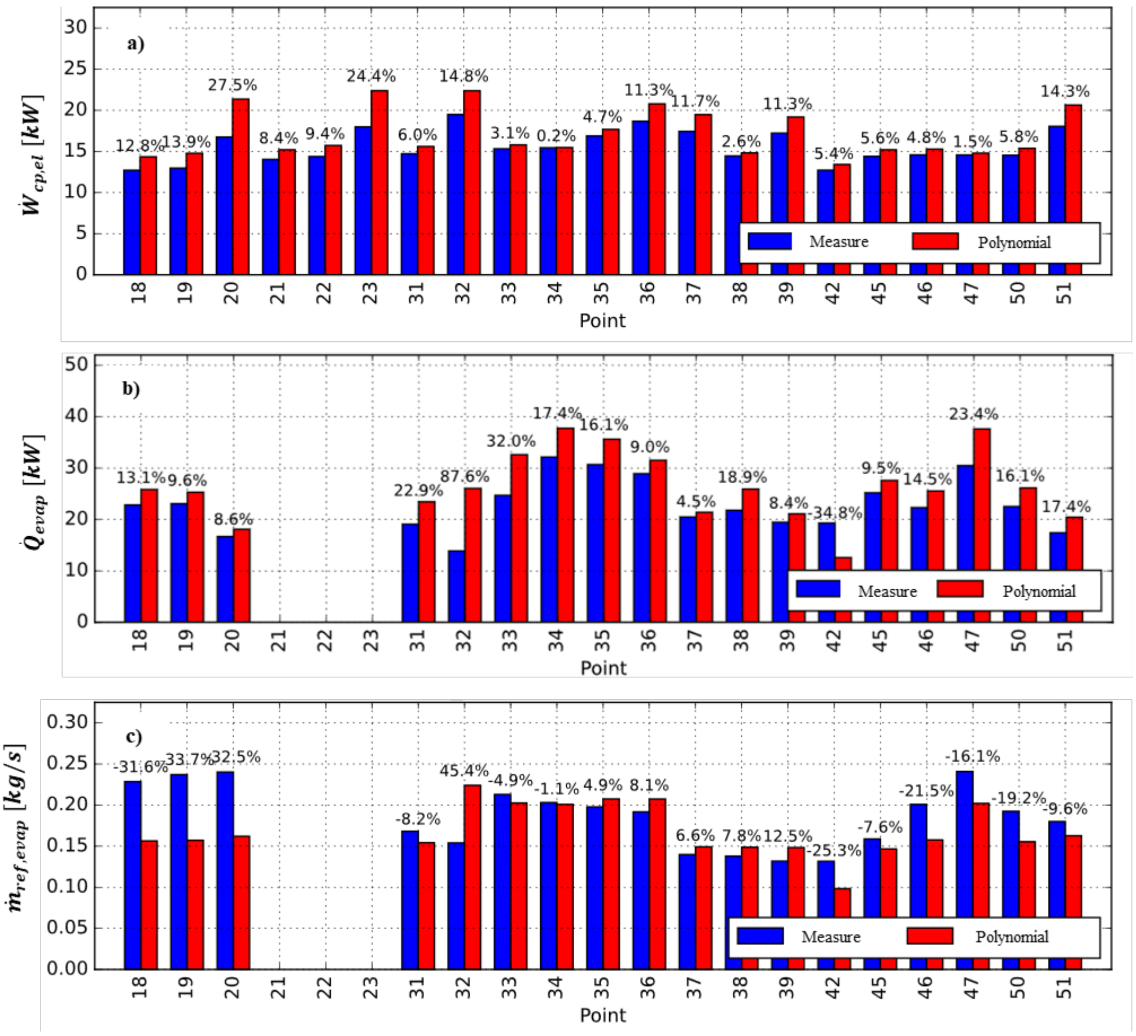

Figure 9: Comparison between manufacturer polynomial and measured values for compressor electric power (a), Cooling Capacity (b), and evaporator refrigerant mass flow rate (c).

In Figure 10 and 11, a scatter plot shows measured electric consumption and cooling capacity as a function of source inlet temperature and sink outlet temperature. The graph shows how electricity consumption is strongly dependent on hot water temperature, exceeding 15 kW when the sink outlet is around 130 °C for all configurations. Minimum electricity consumption is 7 kW, measured when water temperature is at 35/70 °C (cold water inlet/hot water outlet).

Concerning cooling capacity, given an evaporator inlet temperature cooling capacity is maximum when hot water outlet is minimum. Moreover, maximum cooling capacity, close to 28/30 kW, is reached in points 65/120 °C and 50/90 °C.

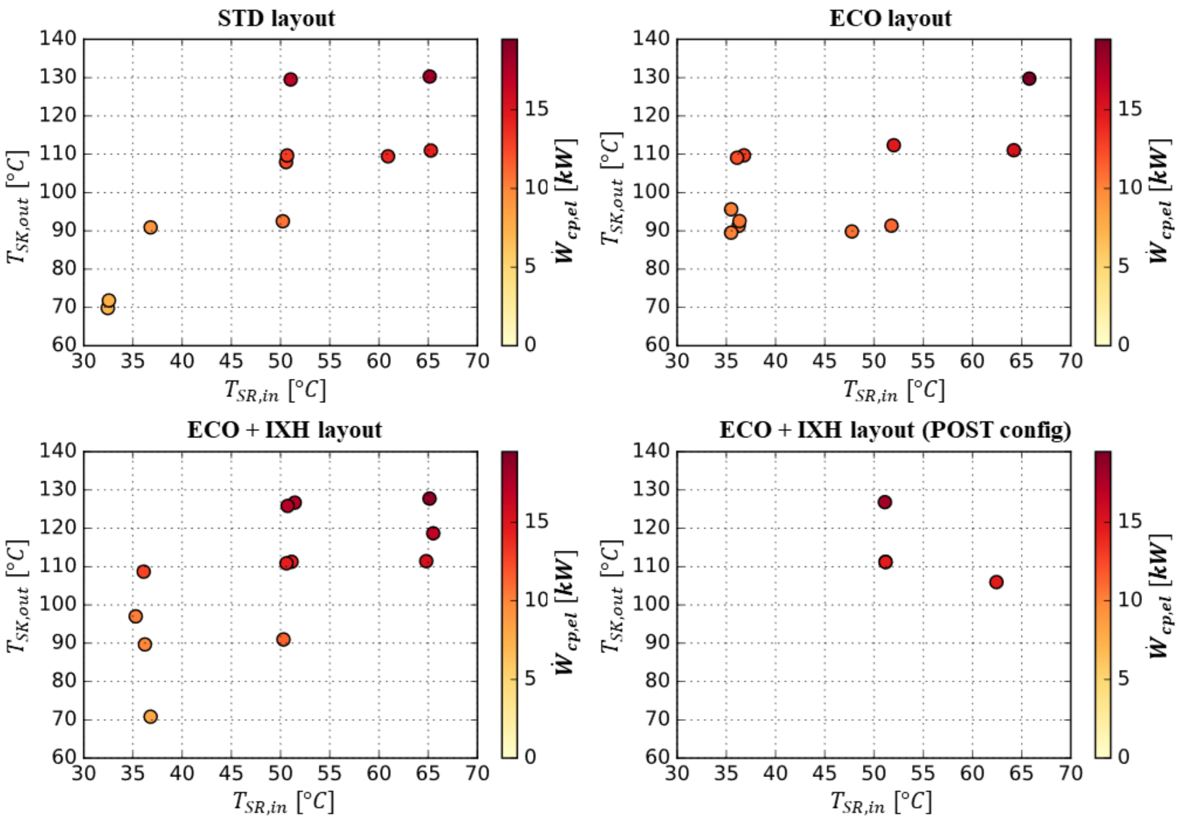

Figure 10: Compressor power overview for different layout as function of source inlet temperature and sink outlet temperature

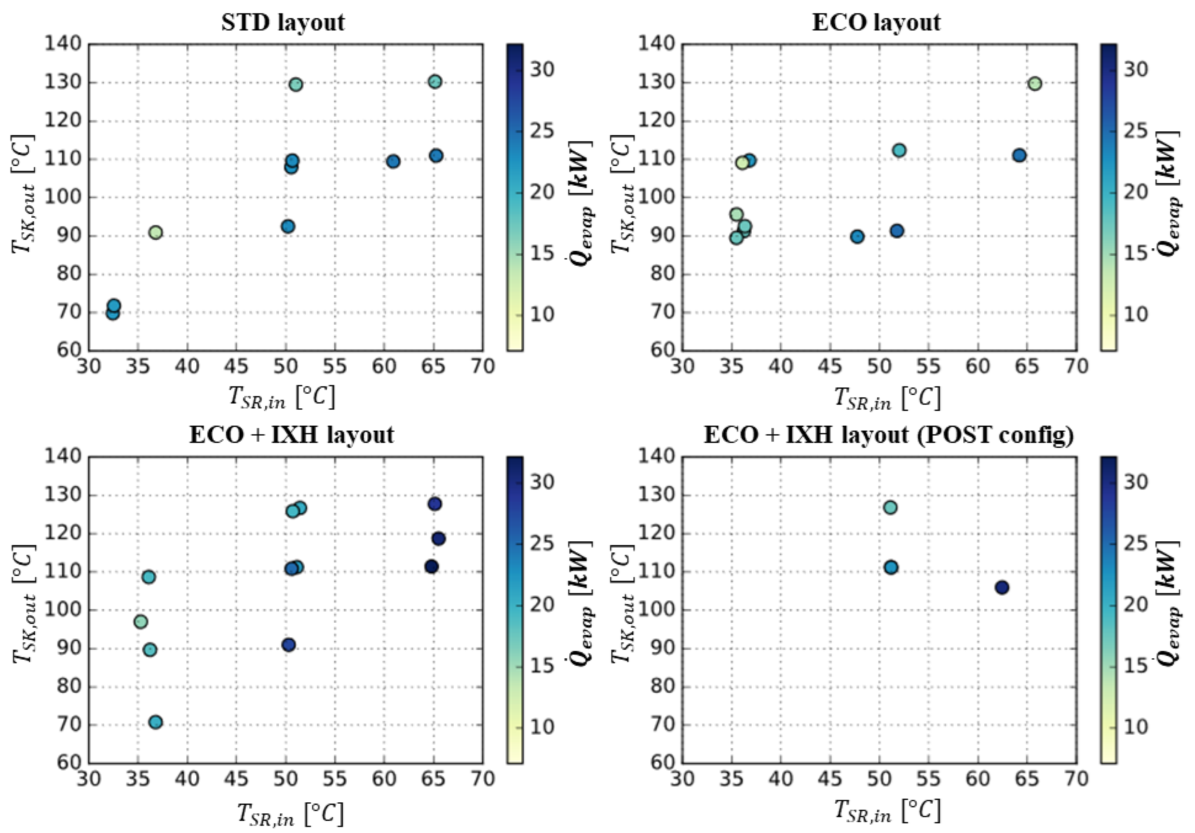

Figure 11: Cooling capacity overview for different layout as function of source inlet temperature and sink outlet temperature

Figure 12 shows final heating capacity and COP comparison for different configurations. Derived heating capacity is calculated by summing measured cooling capacity and electric consumption (as mentioned before hot side mass flow rate measurement was not stable for all tests). The yellow, orange, and red columns refer to source inlet temperatures of 35, 50, and 65 °C, respectively. This result outlines the beneficial role of the regenerator, especially when the source temperature is higher than 50 °C (most likely working condition). In fact, both heating capacity and COP increase when considering both regenerator and economizer. With this configuration, heating capacity reaches 47 kW at 65/130 °C, and in all configurations where the source inlet temperature is higher than 50 °C, COP is greater than 2.2. Controlling the expansion valve via superheating after the regenerator (POST configuration) does not strongly affect results compared to standard regenerator functionality, but it reduces compressor inlet superheating and results in a lower compressor outlet temperature. For this reason, this configuration can be used when working close to the maximum compressor outlet temperature (160 °C).

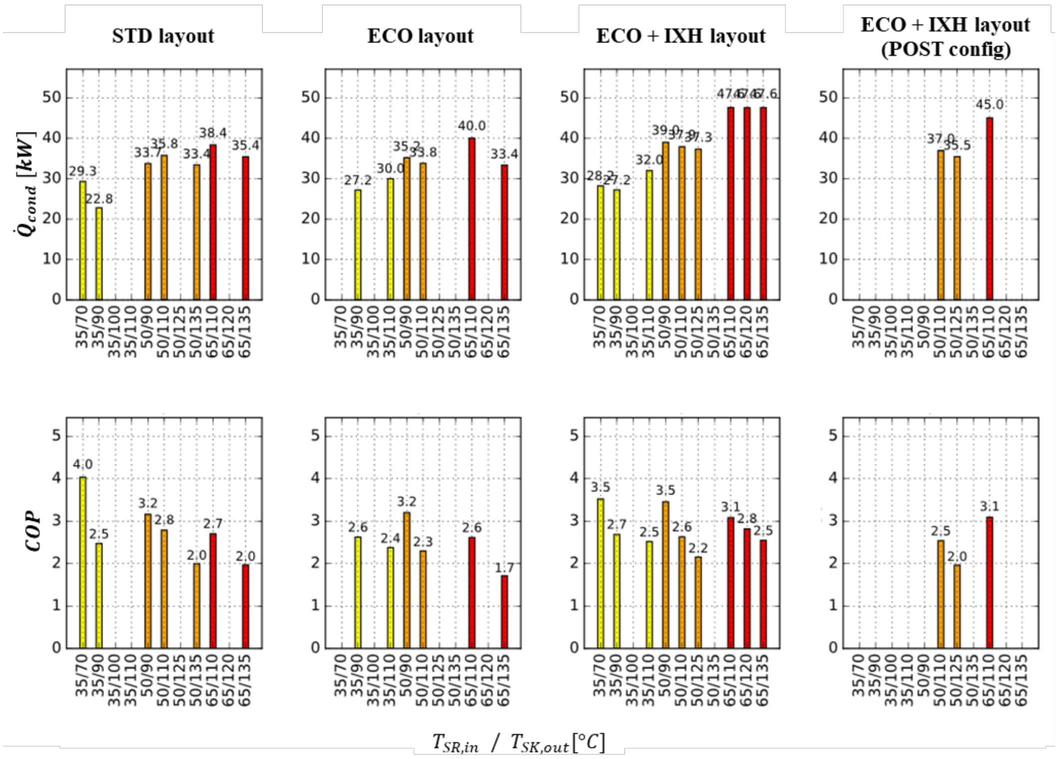

Figure 12: Derived heating capacity overview and COP results for different layout as function source of inlet temperature and sink outlet temperature

4. Conclusions

The integration of a TCM-based seasonal TES requires HTHPs capable of achieving output temperatures above 120 °C, depending on the behaviour of the adopted thermochemical material. The inclusion of auxiliary components, namely an economiser and an internal regenerative heat exchanger, demonstrated numerically clear performance benefits. When both were employed, the COP improved by over 25% for secondary mass flow rates around 30%. The economiser proved effective in reducing the power consumption of the first compression stage while maintaining acceptable compressor discharge temperatures. These findings underline the importance of properly selecting compressors suitable for such transformations, given the limitations imposed by flow diversion and oil degradation at high discharge temperatures.

Experimental tests on the HTHP prototype confirmed the consistency between the numerical model and the measured performance. Data filtering and validation procedures ensured the reliability of the test results, excluding unstable operating conditions or incorrect valve operation. The comparison between measured data and compressor manufacturer polynomials showed good agreement, with measured electric consumption and cooling capacity generally slightly lower than the predicted values, typically within a 15% deviation. The performance mapping revealed that electric consumption increases with hot water outlet temperature, reaching about 15 kW at 130 °C, while cooling capacity reaches up to 28–30 kW under conditions of 65/120 °C and 50/90 °C (evaporator/condenser). The derived heating capacity achieved up to 47 kW in the 65/130 °C configuration, and COP values exceeded 2.2 for evaporator inlet temperatures above 50 °C. Finally, the combined use of economiser and regenerator enhanced both heating capacity and efficiency, confirming the benefit of advanced cycle architectures for high-temperature applications. The POST configuration, which controls expansion based on post-regeneration superheating, further stabilised compressor operation by lowering the discharge temperature, useful when operating near technical limits.

Overall, the results validate the proposed HTHP concept and its integration with the innovative DC cooling and storage systems.

The device will undergo further experimental testing in additional setups and research laboratories prior to deployment at the demo site. Advanced exergetic and exergoeconomic analyses will be carried out in the future to assess the economic viability of adopting performance-enhancing components, whose benefits have so far been demonstrated in this case exclusively from a thermodynamic perspective.

Nomenclature

cond	Condensation / condenser	SR	Source
ECO	Economiser	SK	Sink
evap	Evaporation /evaporator	STD	Standard
HTHP	High temperature heat pump	WHR	Waste heat recovery
IHX	Internal heat exchanger		

Acknowledgements

Funding from the Horizon Europe Project THUNDER - THermochemical storage Utilisation eNabling Data centre seasonal Energy Recovery (Horizon Europe Programme– Call CL5-2023-D3-01 - G.A. No. 101136186).

References

[1] Socci, L, Rocchetti A., Verzino A., Zini A., Talluri L., Enhancing Third-Generation District Heating Networks with Data Centre Waste Heat Recovery: Analysis of a Case Study in Italy. Energy 313:134013, 2024

[2] Zini A, Socci L., Vaccaro G., Rocchetti A., Talluri L. 2024. Working Fluid Selection for High-Temperature Heat Pumps: A Comprehensive Evaluation, Energies 17 (7): 1556, 2024

[3] Wahlroos, M., Pärssinen M., Manner J., Syri S, Utilizing Data Center Waste Heat in District Heating – Impacts on Energy Efficiency and Prospects for Low-Temperature District Heating Networks, Energy 140:1228–38, 2017

[4] Horizon Europe Project THUNDER - THermochemical storage Utilisation eNabling Data centre seasonal Energy Recovery (Horizon Europe Programme– Call CL5-2023-D3-01 - G.A. No. 101136186) – Accssible website: *https://www.thunderproject.eu/*

[5] Glüge, J, Breuer K., Hafner A., Vering C., Müller D., Cousins I.T., Lohmann R., Goldenman G., Scheringer M., Finding Non-Fluorinated Alternatives to Fluorinated Gases Used as Refrigerants. Environmental Science: Processes & Impacts 26 (11): 1955–74, 2024

[6] Pérez-Peña, M.P., Fisher J.A., Hansen C., Kable S.H., Assessing the Atmospheric Fate of Trifluoroacetaldehyde (CF3 CHO) and Its Potential as a New Source of Fluoroform (HFC-23) Using the AtChem2 Box Model». Environmental Science: Atmospheres 3 (12): 1767–77, 2023

[7] Arpagaus, C and Bertsch S.S., Experimental Results of HFO/HCFO Refrigerants in a Laboratory Scale HTHP with up to 150 °C Supply Temperature, 2nd Conference on High Temperature Heat Pumps, 9th September 2019, Copenhagen, Denmark, 2019

[8] Arpagaus, C., Bless F., Uhlmann M., Schiffmann J., Bertsch S.S., High Temperature Heat Pumps: Market Overview, State of the Art, Research Status, Refrigerants, and Application Potentials. Energy 152, 985–1010, 2018

[9] Lemmon E.W., Huber M.L., McLinden M.O., NIST Standard Reference Database 23: Reference Fluid Thermodynamic and Transport Properties-REFPROP, Version 10